Biosensors and Bioelectronics 142 (2019) 111535

Contents lists available at ScienceDirect

Biosensors and Bioelectronics

journal homepage: www.elsevier.com/locate/bios

Ti_3C_2/Cu_2O heterostructure based signal-off photoelectrochemical sensor for high sensitivity detection of glucose

Mingxia Li, Haiyan Wang, Xiaoxia Wang, Qiujun Lu, Haitao Li, Youyu Zhang*, Shouzhuo Yao

Key Laboratory of Chemical Biology and Traditional Chinese Medicine Research (Ministry of Education), College of Chemistry and Chemical Engineering, Hunan Normal University, Changsha, 410081, PR China

ARTICLE INFO

Keywords:
Photoelectrochemical sensor
Non-enzymatic
Ti_3C_2/Cu_2O heterostructure
O_2 sensitive
Glucose detection

ABSTRACT

Photoelectrochemical (PEC) sensing has emerged as a simple and practical method for the analysis and detection, its separated optical signal and detection electrical signal give it the advantages of reduced background noise and outstanding sensitivity. Here, we synthesized a Ti_3C_2/Cu_2O composite through simple oil bath heating process, whose excellent PEC performance and sensitive photoelectric response to glucose make it a propitious substitution to glucose oxidase. On this basis, we construct a PEC non-enzymatic sensor based on the Ti_3C_2/Cu_2O heterostructure for the detection of glucose. Under the optimal conditions, the photocurrent of Ti_3C_2/Cu_2O is linear with the logarithm value of glucose concentration in the wide range of 0.5 nM to 0.5 mM with a detection limit of 0.17 nM. Furthermore, the successful detection of glucose in standard samples and human serum by the proposed Ti_3C_2/Cu_2O based PEC non-enzymatic sensor demonstrates the application prospect of heterostructure material in PEC sensor, which provides a new thought for the design and construction of PEC non-enzymatic sensing platform.

1. Introduction

Glucose is an indispensable component in human body, providing energy for cell metabolism and ensuring normal work of body functions. In addition, glucose in blood is a clinical indicator of diabetes, excess or deficiency will induce diabetes and hypoglycemia, respectively (Gopalan et al., 2017). Thus, quantitative determination of glucose in blood serum is of great meaningfulness. To date, researches on glucose detection have been varied and mature, such as fluorometric (Liu et al., 2015b), colorimetric (Li et al., 2018), electrochemical (Chaiyo et al., 2017) and photoelectrochemical methods (Dai et al., 2017). Among these detection methods, glucose oxidase is adopted for its outstanding selectivity and sensitivity. Unfortunately, the limitations of glucose oxidase in terms of storage, cost, reproducibility and chemical stability have affected the practical application of biosensors to some extent. Recent years, various nanomaterials have been studied as the substitution to glucose oxidase to construct non-enzymatic glucose sensors (Nallal et al., 2017). The widely studied non-enzymatic methods are simple in operation and low in cost, but still suffer from one or more weaknesses of low sensitivity and poor selectivity. Therefore, the exploration of a non-enzymatic method with high sensitivity and selectivity toward glucose detection has been an urgent concern.

MXenes is a novel family of 2D transition-metal carbides and/or carbonitrides material, which has ignited much interest of researchers since it was prepared. Gogotsi and his group obtained the Ti_3C_2 via etching away Al from Ti_3AlC_2 using aqueous HF solution in room temperature, and thus, the formation of this new 2D material was reported since then (Naguib et al., 2011). Ti_3C_2 was one of the most widely used MXenes, exhibiting a variety of distinguished properties including good conductivity, small diffusion barrier, high volumetric capacitance and superior photothermal conversion efficiency, which make it a promising material in energy storage (Anasori et al., 2017), lithium ions batteries (Er et al., 2014), cell imagining (Xue et al., 2017) and photothermal treatment (Li et al., 2017; Liu et al., 2017). Obviously, Ti_3C_2 is mainly applied in the field of electrochemistry and photochemistry. But Ti_3C_2 also exhibits the potential application prospect in photoelectric fields. For example, the large surface area and exposed metal sites of Ti_3C_2 provide more active sites for the growth of semiconductors (Michael et al., 2014; Zhou et al., 2017). Furthermore, Ti_3C_2 is conductive to the separation and transmission of photo-induced carriers in Ti_3C_2/semiconductor heterostructure because of the built-in electric field formed in the interface of Ti_3C_2 and semiconductor, which is caused by the difference between valance band and Fermi levels (E_F) (Kang et al., 2017; Peng et al., 2016). Particularly, Hefei Wand etc. reported that the OH-functionalized Ti_3C_2 was an excellent electrode

* Corresponding author.
E-mail address: zhangyy@hunnu.edu.cn (Y. Zhang).

https://doi.org/10.1016/j.bios.2019.111535
Received 22 April 2019; Received in revised form 15 July 2019; Accepted 24 July 2019
Available online 24 July 2019
0956-5663/

material for semiconductors to construct heterojunctions whose Schottky barrier nears to zero by first principle calculations (Wang et al., 2017). Zhe Kang etc. prepared $Ti_3C_2T_X$/n-Si Schottky junction heterostructures by van der Waals forces and fabricated a self-driven vertical junction photodetector with high response and recovery speed (Kang et al., 2017). On the basis of the theoretical calculations and experimental researches, it can be concluded that the Ti_3C_2 is anticipated to function as an ideal supporting material in PEC sensors. In addition, the combination of Ti_3C_2 with photoactive material such as semiconductors can well overcome the drawback of the short lifetime of the photo-induced electrons.

Cu_2O, as a nontoxic and abundant p-type semiconductor with narrow bandgap of 2.0-2.2 eV, is much popular in photoelectric material for its broad light harvest range and stable photocurrent (Kecsenovity et al., 2017). But the Cu_2O inevitably has the disadvantage of a high recombination rate of electron-hole pairs, which is the inherent limitation nature of pure semiconductors. Doping with metals and bonding with energy band matched semiconductors are both common and effective strategies to obtain an improvement of charge transfer rate (Lingmei et al., 2015; Wang et al., 2015). Unfortunately, doping methods are suffering from complicated operation and limited economic benefits, while the high contact resistance between photoactive material and electrode limits the migration of electrons. Therefore, it's of great importance to have a contact material combining with Cu_2O to construct a heterostructure in which the migration of electrons is less obstructed.

Herein, the well-defined Ti_3C_2/Cu_2O heterostructure was synthesized by a simple oil bath heating process. Cu_2O with a regular octahedron shape is a photoactive material in the PEC sensing system. After the introduction of Ti_3C_2, the large surface area of Ti_3C_2 offers mounts of active sites for the growth of Cu_2O, thus the prepared Ti_3C_2/Cu_2O heterostructure is of high carrier separation rate, which ultimately results in an enhanced PEC performance compared with pure Cu_2O. Particularly, the Ti_3C_2/Cu_2O was found to be sensitive to dissolved oxygen and the photocurrent of Ti_3C_2/Cu_2O decreased in the presence of glucose due to the consumption of the dissolved O_2 in the redox process of glucose. On this basis, a non-enzymatic PEC sensor based on the Ti_3C_2/Cu_2O heterostructure is constructed for the detection of glucose. The PEC sensor shows a wide range and low detection limit toward glucose and is applied to the detection of human serum successfully.

2. Experimental section

2.1. Reagents and chemicals

HCl, $Cu(CH_3COO)_2{\cdot}H_2O$ and $C_6H_{12}O_6$ were purchased from Shanghai Reagent (Shanghai, China); Aluminum titanium carbide (Ti_3AlC_2) was purchased from Forsman Technology Co., Ltd.; LiF (99.9%) was purchased from Aladdin (Shanghai, China). All other reagents were of analytical grade and without any purification. The ultrapure water used in this work was produced by Millipore Milli-Q water purification system (Millipore, $\geq 18\,M\,cm^{-1}$, U.S.A). The Britton-Robison buffer solution (B-R pH 11.92) was prepared as electrolyte. The human serums were obtained from Hospital of Hunan Normal University.

2.2. Apparatus

The photoelectrochemical measurements were performed on a PEAC 200A PEC reactor (Tianjin ida hengsheng, China) with a 50 W halogen lamp as light resource and photocurrents were recorded by CHI1030C electrochemical workstation. A three-electrode system consists of a saturated Ag/AgCl electrode (sat. KCl), a Pt wire and modified FTO, which serve as reference electrode, counter electrode and working electrode, respectively. The PEC experiments were performed with the open circuit voltage of Ti_3C_2/Cu_2O at a constant potential of 0.06 V (*vs.* saturated Ag/AgCl). Scanning electron microscopy (SEM) images were recorded on a S4800 Scanning electron microscope (Hitachi Ltd, Japan) with a field emission electron gun. X-ray photoelectron spectra (XPS) were performed on K-Alpha 1063 (Thermo Fisher Scientific, America). The X-ray powder diffraction (XRD) images were obtained using a Bruker D8-Advance diffractometer with Cu Kα radiation (λ = 1.5418 Å). Fourier transform infrared (FT-IR) spectra were recorded on a Nicolet Nexus 670 FT-IR spectroscopy (Nicolet Instrument Co., USA). The ultraviolet–visible (UV–vis) DRS spectra were recorded on a U-3310 UV–vis DRS spectrophotometer (Hitachi Ltd, Japan).

2.3. Preparation of Ti_3C_2 and Ti_3C_2/Cu_2O

Typically, the synthesis of Ti_3C_2 was based on the previously reported literature (Ghidiu et al., 2014). Firstly, solution consists of 0.8 g of LiF and 10 mL of 9 M HCl was prepared, after which 0.5 g of Ti_3AlC_2 was added slowly into the aforementioned solution under ice-water bath to avoid drastic local overheating. After stirring for 20 h at 37°C, the product was centrifuged in 3500 rpm for 5 min and washed with deionized water for several times until the pH was approximately neutral. Finally, the product was dried at room temperature to obtain the multi-layered Ti_3C_2.

Next, the Ti_3C_2/Cu_2O nanocomposite was synthesized via a simple oil bath heating reaction. 0.1 g of Ti_3C_2, 0.5 g of $Cu(CH_3COO)_2{\cdot}H_2O$ and certain amount of $C_6H_{12}O_6$ were added into 100 mL of distilled water in 250 mL round-bottomed flask and sonicated for 30 min to obtain a uniformly dispersed suspension. The suspension was heated to 90°C and kept for 6 h. After washing with water and ethanol for several times, the solids were dried in room temperature to obtain the reddish brown product Ti_3C_2/Cu_2O. The pure Cu_2O was prepared with the same method without adding Ti_3C_2.

2.4. Preparation of Ti_3C_2/Cu_2O/FTO electrode

The FTO were ultrasonic washed with distilled water, acetone, distilled water, ethanol, distilled water each for 15 min in sequence and dried in 60°C for 2 h. 10 mg of the prepared Ti_3C_2/Cu_2O was added to 1 mL of distilled water and ultrasonic for 30 min to make it dispersed evenly. About 100 μL of the slurry was dispersed onto the pretreated FTO in two drops after which the Ti_3C_2/Cu_2O/FTO was dried in 60 °C. The resulting electrode was finally employed as a working electrode in the PEC detection.

3. Results and discussion

3.1. Structure and morphology characterizations of the prepared materials

Scanning electron microscopy (SEM) was performed to investigate the morphology of the as-prepared Ti_3C_2, Cu_2O and Ti_3C_2/Cu_2O. As shown in Fig. 1a, the Ti_3AlC_2 is tightly structured like a rock, while the HF etched-Ti_3C_2 exhibits an organ-like shape, which is consisted of Ti_3C_2 nanosheets (Fig. 1b). The Cu_2O is mainly of octahedral shape (Fig. 1c) with a size about 2 μm (Fig. S1). The high surface area and numerous active sites of Ti_3C_2 allowed the growth of Cu_2O, and the size of Cu_2O on the surface of Ti_3C_2 is getting smaller due to the avoided gathering (Fig. 1d).

The chemical composition of the composite and valance state of element Cu were studied by X-ray photoelectron spectroscopy (XPS). The survey spectrum (Fig. S2a) of the Ti_3C_2/Cu_2O confirmed the existence of Ti, C, Cu and O. The Cu 2p peaks of the Ti_3C_2/Cu_2O were fitted in Fig. 2a. Except for the peaks of Cu^+ located in 932.4 eV and 952.3 eV (Kang et al., 2015; Liu et al., 2015a), peaks centered at 933.5 eV and 953.5 eV were ascribed to Cu^{2+}, which demonstrated the slight oxidation of Cu^+ on the surface and the broad and weak satellite peak at 943.2 eV further confirmed it (Li et al., 2015). In addition, the

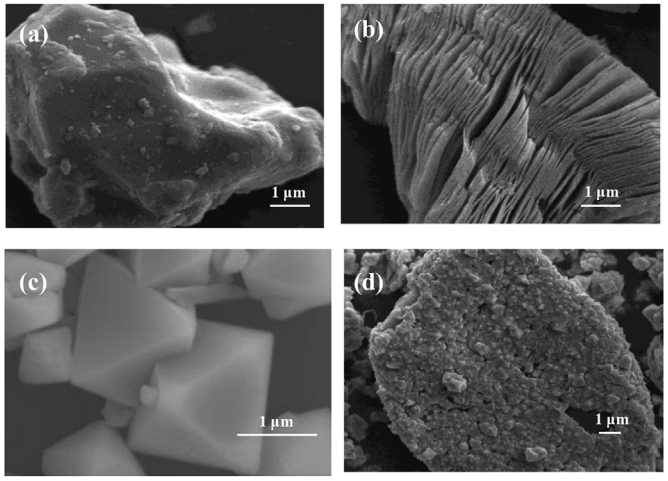

Fig. 1. SEM of (a) Ti_3AlC_2, (b) Ti_3C_2, (c) Cu_2O and (d) Ti_3C_2/Cu_2O.

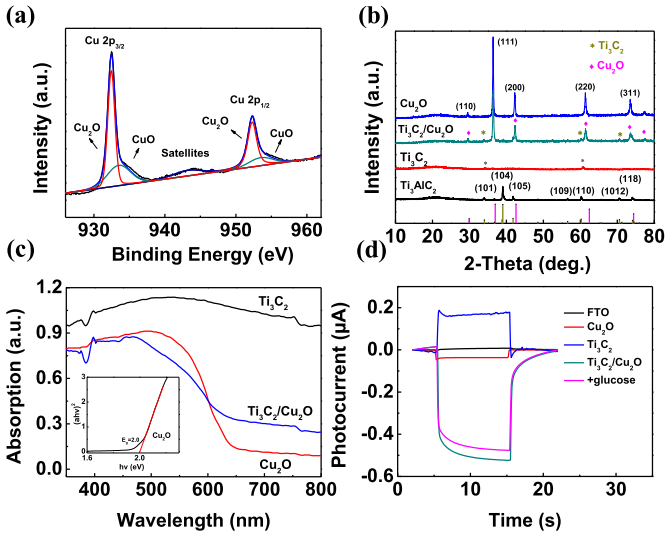

Fig. 2. (a) XPS of Cu 2p in the Ti_3C_2/Cu_2O; (b) XRD of Ti_3AlC_2, Ti_3C_2, Cu_2O and Ti_3C_2/Cu_2O; (c) UV–vis absorbance spectra of Ti_3C_2, Cu_2O and Ti_3C_2/Cu_2O (inset: Tauc Plots $((\alpha h\nu)^2$ *vs.* $h\nu)$ of Cu_2O); (d) Photocurrent of bare FTO, Ti_3C_2/Cu_2O/FTO, Cu_2O/FTO and Ti_3C_2/Cu_2O/FTO in the B-R buffer solution (pH 11.92) and in the presence of 1 μM glucose.

X-ray diffraction (XRD) characterization was further investigated to identify the composition and crystal structure of synthesized composite. As shown in Fig. 2b, the multilayer Ti_3C_2 was etched successfully for the peak of Al at 40° was disappeared (Mashtalir et al., 2013). The diffraction peaks at 29.6°, 36.4°, 43.3°, 61.4° and 73.5° were matched well with the diffraction peaks of the standard card of Cu_2O (Wang et al., 2015). The characteristic diffraction peaks of Ti_3C_2 and Cu_2O appeared in the Ti_3C_2/Cu_2O, indication the successfully prepared of the Ti_3C_2/Cu_2O material.

The FTIR spectra of Ti_3C_2, Cu_2O and Ti_3C_2/Cu_2O composite were shown in Fig. S2b. A broad peak of Ti_3C_2 was observed at 672 cm^{-1}. As for Cu_2O, the peak at 621 cm^{-1} is ascribed to Cu–O vibration (Gao et al., 2012), which can be also observed in Ti_3C_2/Cu_2O composite, suggesting the successfully connection between Ti_3C_2 and Cu_2O.

The light harvesting capacity of the multilayered Ti_3C_2, octahedral Cu_2O and the nanocomposite Ti_3C_2/Cu_2O was demonstrated on the UV–vis diffuse reflectance spectrum (DRS) in Fig. 2c. Ti_3C_2 shows no obvious absorption edge in the range from 200 to 800 nm for the metallic property. The absorption edge of Cu_2O is located at 650 nm, exhibiting its excellent visible light absorption capacity. Furthermore, it can be seen from the picture that the light absorption capacity of the composite after introducing Ti_3C_2 is superior to that of pure Cu_2O. The bandgap of Cu_2O is calculated through Kubelka-Munk function (inset of Fig. 2c) and the position of conductive band (CB) and valance band (VB) are determined according to the transformed Tauc plots and empirical formula (supporting information) (Kecsenovity et al., 2017). The E_g of Cu_2O is calculated to be 2.0. E_{CB} and E_{VB} (-0.17 and 1.83 eV *vs.* SHE, respectively) can be converted to be 0.07 and 2.07 eV (*vs.* NHE) according to the Nernst equation (Yang et al., 2017). The original Fermi level (E_F) of Ti_3C_2 is 1.88 eV (*vs.* NHE) (Ran et al., 2017). While the intimate contact between Ti_3C_2 and Cu_2O accompany with the rising E_F of Ti_3C_2 is propitious to the transfer of holes from Cu_2O to Ti_3C_2 (Jinhui et al., 2013; Liu et al., 2019), thus obtaining the enhanced separation rate of photo-induced carriers.

3.2. Characteristics of PEC sensing

The PEC activity of the Ti_3C_2/Cu_2O was studied by transient photocurrent detection. As exhibited in Fig. 2d, the Cu_2O as p-type semiconductor showed relatively weak stable cathode photocurrent under irradiation of visible light source, obviously because the relatively narrow band gap made it easy for the electrons and holes to recombine. The pure Ti_3C_2 exhibited an anode photocurrent, while after the introduction of Cu_2O, an obviously enhanced cathode photocurrent of Ti_3C_2/Cu_2O is observed compared with pure Cu_2O. Owing to the low work function (Liu et al., 2016b) derived from good metallic conductivity and high carrier mobility of the multi-layered Ti_3C_2, the photo-induced holes on the valance band (VB) of Cu_2O are transport to electrode through Ti_3C_2 rapidly, therefor promoting the charge separation and obtaining a stronger photocathode current.

In order to figure out whether the enhanced photocurrent of Ti_3C_2/Cu_2O is due to the better charge separation, the photoluminescence (PL) spectra and electrochemical impedance spectroscopy (EIS) were introduced. Generally, the PL intensity is assigned to the radiative recombination of photo-induced charges (Luo et al., 2016), the lower the fluorescence intensity, the higher the separation rate of electrons and holes (Zhou et al., 2018). As shown in Fig. 3a, the peak intensity of Ti_3C_2 (Fig. S4) and Cu_2O was significantly higher than that of Ti_3C_2/Cu_2O, which mean that migration of photo-induced carriers was exist

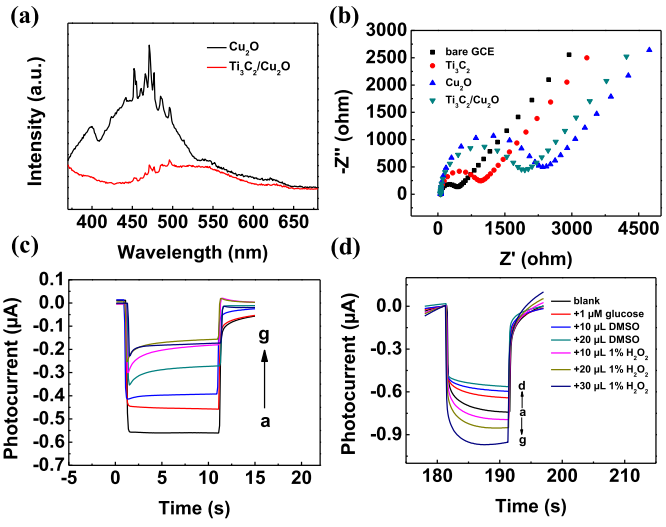

Fig. 3. (a) Photoluminescence spectra of Cu_2O and Ti_3C_2/Cu_2O; (b) Nyquist diagrams of bare GCE, Ti_3C_2/GCE, Cu_2O/GCE and Ti_3C_2/Cu_2O/GCE in 2 mM Fe $(CN)_6^{3-/2-}$ + 0.1 M K_2SO_4; (c) Photocurrent responses of the Ti_3C_2/Cu_2O electrode after deoxygenation with N_2 for 0, 1, 3, 5, 10, 20, 30 min (from curves a to g) in the electrolyte containing 1 μM glucose; (d) Photocurrent of Ti_3C_2/Cu_2O/FTO in the absence (a) and presence (b) of 1 μM glucose, Ti_3C_2/Cu_2O/FTO after the addition of DMSO (b-d) and H_2O_2 (e-g)in the B-R buffer solution (pH 11.92).

and resulted in a higher charge separation rate. Furthermore, the EIS spectra in Fig. 3b auxiliary analyzed the charge transfer situation. Generally, the arc radius is represents the charge transfer impedance between the material and electrolyte, in which a smaller arc represents a faster charge transfer. Obviously, the Ti_3C_2/Cu_2O has a smaller radius compared with that of Cu_2O, suggesting the apparently increased charge transfer efficiency on the surface of Ti_3C_2/Cu_2O. Oppositely, the photocurrent of Ti_3C_2/Cu_2O prepared through electrodeposition is weaker than that of Cu_2O/FTO (Fig. S5), indicating that the cathode photocurrent of Cu_2O will be partly counteracted by the anode photocurrent of Ti_3C_2 if charge transfer mechanism can't be established.

In addition, the smaller size of octahedral Cu_2O after connecting with Ti_3C_2 provides a shorter path for electrons to move to the surface of photocathode, resulting in a reduced recombination probability of electrons and holes (Zhang et al., 2017). Furthermore, the much higher surface area because of the multi-layered Ti_3C_2 broadens the absorption area of visible light, which can be observed in Fig. 2c. Therefore, we conclude that the enhanced photocurrent of composite comes from the smaller size and higher surface of Cu_2O, as well as the separated charge caused by the transfer mechanism between Ti_3C_2 and Cu_2O.

3.3. Sensing mechanism of Ti_3C_2/Cu_2O sensing system

According to the energy levels of Cu_2O and reactive oxygen species (ROS) formation potential (-0.33 V) and O_2/H_2O potential (Liu et al., 2016a), the Ti_3C_2/Cu_2O might react with O_2 and transport the electrons to the dissolved O_2 in electrolyte. Namely, the ambient O_2 is function as electron acceptor to help transfer the electrons and facilitates the electrons separation. To validate the assumption, the sensitivity of the Ti_3C_2/Cu_2O photocathode to the dissolved O_2 was tested. Under the relatively low OCP condition, air-saturated electrolyte containing glucose was deoxygenated through filling with high pure nitrogen (N_2) as shown in Fig. 3c. The photocurrent decreased with the extension of purging time and reached a minimum at 20 min, indicating that the ambient O_2 was acted as electron acceptor contributed to the enhanced photocurrent. When dissolved oxygen was purged by N_2, the transfer path of electrons to O_2 in electrolyte was prohibited accompany with increased recombination rate of the electrons and holes, eventually resulting in a suppressed photocurrent. The oxygen reduction reaction is shown in equation of (Juodkazytė et al., 2014; Zheng et al., 2016):

$$O_2 + e^- \rightarrow O_2^{\cdot -} \quad (1)$$

$$2O_2^{\cdot -} + 2H_2O \rightarrow H_2O_2 + 2OH^- \quad (2)$$

$$H_2O_2 + e^- \rightarrow 2OH^- \quad (3)$$

In order to further certify the assumption, a comparative experiment was carried out. As shown in Fig. 3d, the photocurrent of Ti_3C_2/Cu_2O increased with the increased volume of 1% H_2O_2, indicating the further reduction of H_2O_2 to H_2O on the photocathode consumed the electrons and resulted to the increased photocurrent. Whilst when small quantity of DMSO was added into the electrolyte as scavenger of $O_2^{\cdot -}$, the photocurrent was obviously decreased (Wang et al., 2019). Obviously, the partial reduced species of oxygen (H_2O_2) was contributed to the sensing process, which was consumed by glucose and thereby obtained a decreased cathode photocurrent (Zanatta et al., 2016).

On the basis of results from the two experiments, the mechanism of the glucose sensing is shown in Scheme 1. Under the irradiation of visible light, the electrons in the VB of Cu_2O are excited to the CB and the holes are generated in the VB. Due to the metallic property of Ti_3C_2, its low work function (varied from 2 eV to 6 eV) enable it acts as hole mediator, allowing for the flow of holes transfer from the p-type Cu_2O to Ti_3C_2. Meanwhile, the dissolved O_2 acts as electron acceptor to transfer the electrons to the electrolyte. Both the electron and hole transfer paths greatly enhance the separation rate of photo-induced carriers, eventually resulting in the enhanced cathode photocurrent. However, when the glucose is added into the electrolyte, the partial reduced species ($O_2^{\cdot -}$, H_2O_2) of O_2 are consumed by glucose. One of the transfer paths of electrons to electrolyte is prohibited in the lack of electron acceptor, eventually resulting in a decreased photocurrent. Therefore, the photocurrent responses of Ti_3C_2/Cu_2O decrease with the increasing glucose concentration.

3.4. Optimization of experimental conditions

The optimization of the synthesis condition of Ti_3C_2/Cu_2O was shown in Fig. S3. The effect of pH of electrolyte was investigated in Fig. S3d. The photocurrent increased with the pH range from 7.0 to 9.0 and leveled out range from 9.0 to 11.92. That might be ascribed to the fact that Cu_2O could generate redox couple Cu (I)/Cu (II) in alkaline solution, the redox progress consumed the electrons and suppressed the recombination of photo-induced carriers. Finally, B-R buffer solution (pH 11.92) was chosen as electrolyte in this work for its more stable and regular photocurrent curve. The amplitude of photocurrent is closely related to the applied potential, a more negative applied potential makes a higher cathode photocurrent, also a larger measuring deviation derived from electronic drift (Zhang et al., 2015). As depicted in Fig. S3e, the photocurrent of the Ti_3C_2/Cu_2O was relatively strong even in 0 V and achieved optimum at -0.1 V. The FTO as working electrode has resistance inherently. In order to counteract the resistance of the FTO electrode, the open circuit voltage (OCP) of 0.06 V was ultimately adopted in the following experiments.

3.5. Analytical performance of Ti_3C_2/Cu_2O PEC sensing system

The analytical performance of Ti_3C_2/Cu_2O as photoactive material was investigated by detecting glucose of different concentrations under the optimal condition. As shown in Fig. 4a, the photocurrent responses of the Ti_3C_2/Cu_2O was decreased with the increasing concentration of glucose in the range from 0.5 nM to 0.5 mM. The corresponding calibration curve demonstrating the linear relationship between photocurrent decrease and logarithm value of glucose concentration with a linear equation of $(I_0–I)/I_0 = 0.021\mathrm{Log}C + 0.525$ was shown in Fig. 4b. (I_0 is the photocurrent of the sensor before adding the glucose, I is the photocurrent while adding the glucose with different concentrations, C is the concentration of glucose.). The LOD was calculated to be 0.17 nM, following the analytical function of LOD = Kσ/S, where σ is the standard deviation of the blank solution (n = 10), S is the slope of regression line, K is used as 3 (MacDougall et al., 1980).

The reasons account for the low detection limit and wide detection range probably arise from: (i) the separated light source and detection electrical signal of the PEC sensor enable the low background noise and high sensitivity; (ii) the high charge transfer efficiency of Ti_3C_2 contributes to the separated electron-hole pairs and high specific surface area allows for the loading of numerous Cu_2O; (iii) the octahedral structure of Cu_2O has increased surface area for electro-catalysis and the smaller size after connecting with Ti_3C_2 shortens the electrons transfer distance. In brief, the high surface area and charge transfer mechanism between well-ordered lamellar Ti_3C_2 and homogeneously distributed Cu_2O on the surface contributes to the excellent performance of the PEC sensor.

3.6. Selectivity and stability of the Ti_3C_2/Cu_2O sensor

The selectivity of the Ti_3C_2/Cu_2O sensing system was explored by adding 10 μM of interfering species coexisting in human blood serum into electrolyte (pH 11.92). As shown in Fig. 4c, no significant signal changes in photocurrent were observed compared to the background photocurrent after the addition of 10 μM of ascorbic acid (AA), uric acid (UA), dopamine (DA), lactose, fructose, and sucrose, respectively. While, no apparently change happened in the photocurrent after the addition of mixture containing 1 μM of glucose and 10 μM of interfering

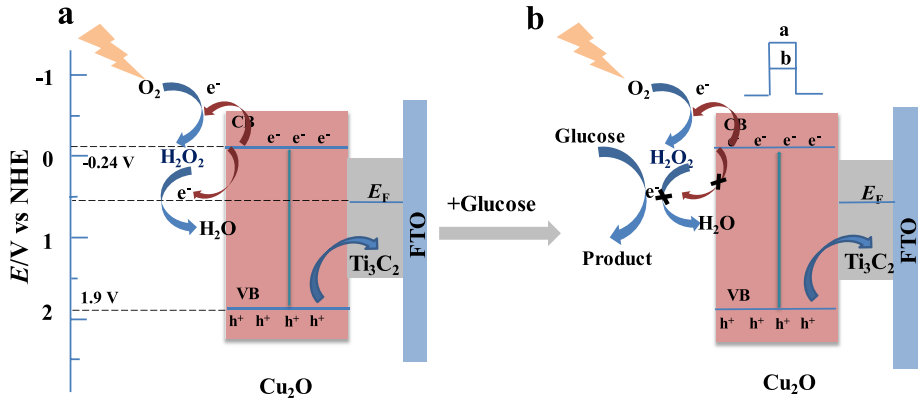

Scheme 1. The charge separation and transfer in the proposed Ti_3C_2/Cu_2O photocathode under visible light (a) and the mechanism illustration of the Ti_3C_2/Cu_2O PEC sensor toward glucose (b).

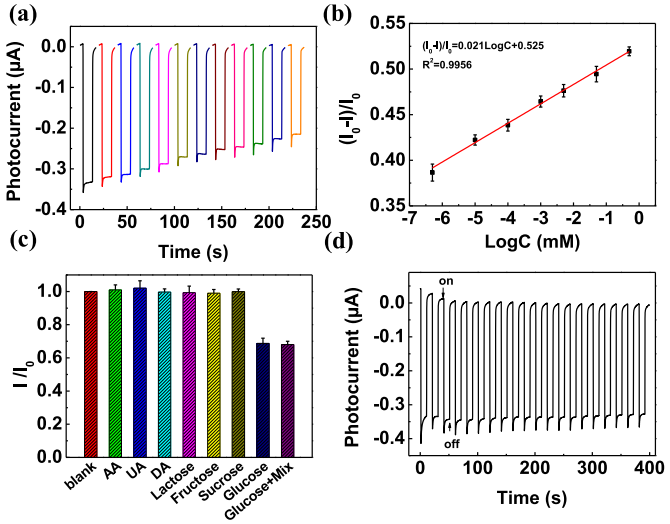

Fig. 4. (a) Photocurrent responses of Ti_3C_2/Cu_2O in the presence of glucose with different concentrations; (b) Corresponding linear relationship between $(I_0–I)/I_0$ and logarithm value of glucose concentration; (c) Photocurrent responses of Ti_3C_2/Cu_2O in B-R buffer solution (pH 11.92) containing 10 μM of co-exiting species (AA, UA, DA, Lactose, Fructose, and Sucrose), 1 μM of glucose and interfering species mixture added in glucose, respectively; (d) Photocurrent stability of the Ti_3C_2/Cu_2O in B-R buffer solution (pH 11.92) containing 1 μM glucose under repeated visible light irradiation.

specie compared with only glucose (1 μM), showing the good selectivity and anti-interference of the Ti_3C_2/Cu_2O sensing system. The good selectivity of the sensor is concerned to the electronic structure of photocathode and O_2 sensitive mechanism of the sensor. Due to the charge generation/transfer mechanism of p-type semiconductor Cu_2O and holes conductor Ti_3C_2, the photo-induced holes are transferred to Ti_3C_2 under the driving force, avoiding the interaction of co-existing interfering species with holes (Wang et al., 2014). Besides, the alkaline electrolyte converts the phenolic hydroxyl and imino group of AA, UA, and DA to deprotonated phenolic hydroxyl and imino group, which are difficult to be oxidized under the relatively low open circuit potential (Li et al., 2015).

Furthermore, it could be observed from Fig. 4d that Ti_3C_2/Cu_2O electrode shown a stable and reproducible photocurrent in electrolyte containing 1 μM of glucose under intermittent visible light irradiation for 400 s, indicating a well-behaved stability.

3.7. Applications in real samples

The feasible of the Ti_3C_2/Cu_2O sensing system for real samples was conducted in human blood serum through recovery experiments as presented in Table 1. After diluted to the specific concentration with B-R buffer solution, the recoveries of glucose detection in serums were determined range from 99%, 101% and 102%, respectively, showing the feasibility of the PEC detection in the detection of biological samples. In addition, the detection of diluted human serum was shown in Fig. S6, indicating the potential of the sensor for its application in the clinical diagnostic of glucose detection.

Table 1
Ti_3C_2/Cu_2O non-enzymatic PEC sensor applied in real sample.

Samples	Determination (μM)	Added (μM)	Detected (μM)	Recovery (%)	RSD (%)
1	3.44 ± 1.6	6	9.38 ± 0.5	99	5.3
2	3.02 ± 1.8	20	23.40 ± 0.8	102	3.4
3	2.82 ± 1.2	30	33.01 ± 1.1	101	2.6

4. Conclusion

In summary, Ti_3C_2/Cu_2O heterostructure has been synthesized through simple oil bath heating method and utilized to construct a non-enzymatic PEC sensor for the glucose detection. Due to the introduction of Ti_3C_2, the recombination of photo-induced charge carriers was hindered, thus the PEC performance of Ti_3C_2/Cu_2O was significantly improved compared with pure Cu_2O. Therefore, the optimized Ti_3C_2/Cu_2O was employed as photocathode because of its enhanced PEC performance and sensitivity to dissolved O_2. The competitive consumption of dissolved O_2 during the redox process of glucose resulted in a reduced photocurrent. Meanwhile, the PEC non-enzymatic sensor exhibited high selectivity and excellent sensitivity for the detection of glucose in model solution and biological samples. In this work, the Ti_3C_2/semiconductor based heterostructure was first used as photocathode for the construction of PEC non-enzymatic sensor, which demonstrated the enormous potential of Ti_3C_2/semiconductor in PEC fields. We believe that our study could arouse the research interest of Ti_3C_2 in PEC application and provide new thoughts for the design of PEC non-enzymatic sensors as well as biosensors.

CRediT authorship contribution statement

Mingxia Li: Investigation, Writing - original draft. **Haiyan Wang:** Data curation. **Xiaoxia Wang:** Methodology. **Qiujun Lu:** Writing - review & editing. **Haitao Li:** Project administration. **Youyu Zhang:** Funding acquisition, Conceptualization, Writing - review & editing. **Shouzhuo Yao:** Project administration.

Acknowledgements

This work was supported by the National Natural Science Foundation of China (21874042 and 21675051), and the Foundation of the Science & Technology Department of Hunan Province (2016SK2020).

Appendix A. Supplementary data

Supplementary data to this article can be found online at https://doi.org/10.1016/j.bios.2019.111535.

References

Anasori, B., Lukatskaya, M.R., Gogotsi, Y., 2017. Nat. Rev. Mater. 2, 16098.
Chaiyo, S., Mehmeti, E., Siangproh, W., Hoang, T.L., Hai, P.N., Chailapakul, O., Kalcher, K., 2017. Biosens. Bioelectron. 102, 113–120.
Dai, W.X., Zhang, L., Zhao, W.W., Yu, X.D., Xu, J.J., Chen, H.Y., 2017. Anal. Chem. 89, 8070–8078.
Er, D., Li, J., Naguib, M., Gogotsi, Y., Shenoy, V.B., 2014. Appl. Mater. Inter. 6, 11173–11179.
Gao, Z., Liu, J., Xu, F., Wu, D., Wu, Z., Jiang, K., 2012. Solid State Sci. 14, 276–280.
Ghidiu, M., Lukatskaya, M.R., Zhao, M.Q., Gogotsi, Y., Barsoum, M.W., 2014. Nature 516, 78–81.
Gopalan, A.I., Muthuchamy, N., Lee, K.P., 2017. Biosens. Bioelectron. 89, 352–360.
Jinhui, Y., Donge, W., Hongxian, H., Can, L., 2013. Accounts Chem. Res. 46, 1900–1909.
Juodkazytė, J., Šebeka, B., Savickaja, I., Jagminas, A., Jasulaitienė, V., Selskis, A., Kovger, J., Mack, P., 2014. Electrochim. Acta 137, 363–371.
Kang, Z., Ma, Y., Tan, X., Zhu, M., Zheng, Z., Liu, N., Li, L., Zou, Z., Jiang, X., Zhai, T., Gao, Y., 2017. Adv. Electron. Mater. 3, 1700165.
Kang, Z., Yan, X., Wang, Y., Bai, Z., Liu, Y., Zhang, Z., Lin, P., Zhang, X., Yuan, H., Zhang, X., 2015. Sci. Rep. 5, 7882.
Kecsenovity, E., Endrodi, B., Toth, P.S., Zou, Y., Dryfe, R.A.W., Rajeshwar, K., Janaky, C., 2017. J. Am. Chem. Soc. 139, 6682–6692.
Li, H., Li, J., Chen, D., Qiu, Y., Wang, W., 2015. Sens. Actuators B Chem. 220, 441–447.
Li, R., Zhang, L., Shi, L., Wang, P., 2017. ACS Nano 11, 3752–3759.
Li, W., Lu, S., Bao, S., Shi, Z., Lu, Z., Li, C., Yu, L., 2018. Biosens. Bioelectron. 99, 603–611.
Lingmei, L., Weiyi, Y., Wuzhu, S., Qi, L., Jian Ku, S., 2015. ACS Appl. Mater. Interfaces 7, 1465–1476.
Liu, C., Kong, D., Hsu, P.C., Yuan, H., Lee, H.W., Liu, Y., Wang, H., Wang, S., Yan, K., Lin, D., Maraccini, P.A., Parker, K.M., Boehm, A.B., Cui, Y., 2016a. Nat. Nanotechnol. 11, 1098–1104.
Liu, C., Xu, Q., Zhang, Q., Zhu, Y., Ji, M., Tong, Z., Hou, W., Zhang, Y., Xu, J., 2019. J. Mater. Sci. 54, 2458–2471.
Liu, G., Zou, J., Tang, Q., Yang, X., Zhang, Y., Zhang, Q., Huang, W., Chen, P., Shao, J., Dong, X., 2017. ACS Appl. Mater. Interfaces 9, 40077–40086.
Liu, L., Yang, W., Sun, W., Li, Q., Shang, J.K., 2015a. ACS Appl. Mater. Interfaces 7, 1465–1476.
Liu, Y., Xiao, H., Goddard 3rd, W.A., 2016b. J. Am. Chem. Soc. 138, 15853–15856.
Liu, Z., Liu, L., Sun, M., Su, X., 2015b. Biosens. Bioelectron. 65, 145–151.
Luo, Z., Li, C., Zhang, D., Wang, T., Gong, J., 2016. Chem. Commun. 52, 9013–9015.
MacDougall, D., Crummett, W.B., et al., 1980. Anal. Chem. 52, 2242–2249.
Mashtalir, O., Naguib, M., Mochalin, V.N., Dall'Agnese, Y., Heon, M., Barsoum, M.W., Gogotsi, Y., 2013. Nat. Commun. 4, 1716.
Michael, G., Lukatskaya, M.R., Meng-Qiang, Z., Yury, G., Barsoum, M.W., 2014. Nature 516, 78–81.
Naguib, M., Kurtoglu, M., Presser, V., Lu, J., Niu, J., Heon, M., Hultman, L., Gogotsi, Y., Barsoum, M.W., 2011. Adv. Mater. 23, 4248–4253.
Nallal, M., Anantha, G.I., Lee, K.P., 2017. ACS Appl. Mater. Interfaces 9, 37166–37183.
Peng, C., Yang, X., Li, Y., Yu, H., Wang, H., Peng, F., 2016. ACS Appl. Mater. Interfaces 8, 6051–6060.
Ran, J., Gao, G., Li, F.T., Ma, T.Y., Du, A., Qiao, S.Z., 2017. Nat. Commun. 8, 13907.
Wang, G.L., Liu, K.L., Dong, Y.M., Wu, X.M., Li, Z.J., Zhang, C., 2014. Biosens. Bioelectron. 62, 66–72.
Wang, H., Chen, S., Jian, Z., Sun, Z., 2017. J. Phys. Chem. C 121, 25164–25171.
Wang, H., Li, M., Li, H., Lu, Q., Zhang, Y., Yao, S., 2019. Mater. Des. 162, 210–218.
Wang, P., Tang, Y., Wen, X., Amal, R., Ng, Y.H., 2015. ACS Appl. Mater. Interfaces 7, 19887–19893.
Xue, Q., Zhang, H., Zhu, M., Pei, Z., Li, H., Wang, Z., Huang, Y., Huang, Y., Deng, Q., Zhou, J., Du, S., Huang, Q., Zhi, C., 2017. Adv. Mater. 29, 1604847.
Yang, X., Qian, F., Wang, Y., Li, M., Lu, J., Li, Y., Bao, M., 2017. Appl. Catal. B Environ. 200, 283–296.
Zanatta, M., Calvillo, L., Zheng, J., Rizzi, G.A., Durante, C., Giallongo, G., Chirkov, D., Colazzo, L., Marega, C., Gennaro, A., Granozzi, G., 2016. Thin Solid Films 603, 193–201.
Zhang, J., Tu, L., Zhao, S., Liu, G., Wang, Y., Wang, Y., Yue, Z., 2015. Biosens. Bioelectron. 67, 296–302.
Zhang, X., Liu, Y., Dong, S., Ye, Z., Guo, Y., 2017. Ceram. Int. 43, 11065–11070.
Zheng, J., Calvillo, L., Rizzi, G.A., Granozzi, G., 2016. ChemPlusChem 81, 391–398.
Zhou, C., Wang, S., Zhao, Z., Shi, Z., Yan, S., Zou, Z., 2018. Adv. Funct. Mater. 28.
Zhou, W., Zhu, J., Wang, F., Cao, M., Zhao, T., 2017. Mater. Lett. 206, 237–240.